

Chapter 2

MODELING OF THE QWITT DIODE

In the previous chapter we discussed the phenomenon of resonant tunneling and the basic device operation of a QWITT diode. In this chapter small signal and large signal models for the QWITT diode will be developed. These models relate physical device parameters to predicted dc and rf performance. In the subsequent chapters these models will be used to help design optimized QWITT devices for any desired frequency of operation.

Due to the negative differential resistance exhibited by quantum wells, and since tunneling is an inherently fast transport mechanism, resonant tunneling devices have been proposed for use in extremely high frequency oscillators. Encouraging preliminary experimental results for such oscillators have been obtained at millimeter-wave frequencies [20]. The maximum frequency of operation for quantum well oscillators has not yet been established; tunneling time through the barrier layers [46], the time uncertainty relation [47, 48], carrier lifetime in the well [49], and equivalent RC circuit models [36, 50, 51] have all been used to estimate this frequency limit. Although these models indicate the possibility of negative resistance at very high frequencies, the maximum oscillation frequencies and power levels actually achieved to date by quantum well oscillators are lower than those achieved by other negative resistance diodes. Thus, there is considerable interest in optimizing quantum well oscillator structures and in establishing their maximum operating frequency limits.

The quantum well diode with the highest reported frequency of oscillation to date has used moderately doped spacer layers approximately $0.5 \mu\text{m}$ thick on either side of the quantum well region [20, 39, 52]. Such thick spacer layers are expected to produce major effects on device performance. Under normal bias the spacer layer on the cathode side of the quantum well will contribute to the total parasitic series resistance in the device. In contrast, a significant portion of the spacer layer on the anode side of the quantum well may be depleted, resulting in a transit-time delay. In the last chapter we suggested that deliberate exploitation of this depletion region in the anode side spacer layer will enhance the performance of quantum well oscillators [37, 38]. Such oscillators, in which transport through a drift region play a significant role, have been termed quantum well injection transit-time (QWITT) diodes [37]. In fact, the existence of significant depleted regions in the best experimental quantum well oscillators suggests that these structures [20, 39] operate in a QWITT-mode, even in cases where the QWITT structure was not intended. In any case, it is clear that analyses of the performance potential of quantum well oscillators must include the effects of spacer layers.

In this section we present a small-signal analysis of quantum well oscillators with an anode-side depletion layer. This analysis provides a considerable amount of information concerning the optimum design and maximum oscillation frequency of quantum well oscillators. The general approach follows the well-established small-signal theory of conventional transit-time devices. The new contributions of this model are: (a) the influence of a negative injection conductance on a transit-time device is analyzed for the first time; (b) the results are interpreted in terms of optimum device design and maximum frequency of oscillation of quantum well

oscillators; (c) new results and insights are obtained for conventional positive injection conductance; and (d) the performance potential of QWITT diodes is directly contrasted to that of other transit-time devices.

2.1 Small Signal Model

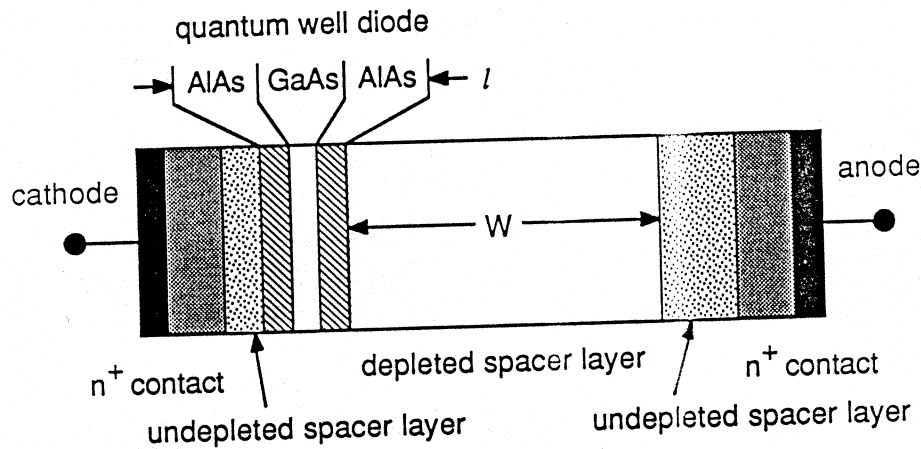
The device structure under consideration is shown in Fig. 2.1(a). It is assumed that the length of the quantum well region, l , is much smaller than the depleted spacer layer length W . The depletion region transit-time is therefore much greater than the transit-time through the quantum well. Transport through the quantum well can be considered instantaneous in this approximation. The quantum well is effectively treated as an injecting cathode whose small-signal equivalent circuit is the 'cold' (geometric) capacitance of the well, in parallel with a conductance which represents the tunneling current (see Fig. 2.1(b)). For small-signal transit-time analysis the injection region (the quantum well here) is characterized by a normalized injection conductance σ , which is given by

$$\sigma = l \left(\frac{\partial J_{\text{QW}}}{\partial V_{\text{QW}}} \Big|_{V_0} \right) \quad (2.1)$$

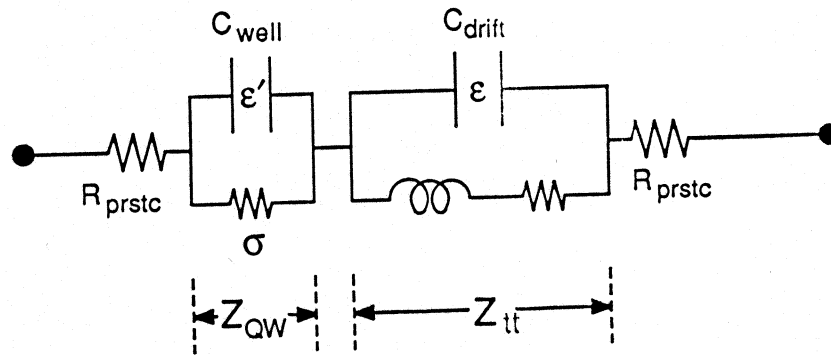
where J_{QW} is the instantaneous current density, V_{QW} is the instantaneous voltage, and V_0 is the dc bias voltage, each across the quantum well region only, excluding the voltage dropped across the depletion region. The specific impedance of the quantum well injection region at an angular frequency ω is then given by

$$Z_{\text{QW}} = \frac{l}{\sigma + j\omega\epsilon} \quad (2)$$

(2.2)



(a)



(b)

Fig. 2.1: (a) Quantum well diode structure which exhibits significant transit-time effects. The GaAs spacer layer on the cathode side of the quantum well region is made thin to reduce parasitic series resistance. A thick, undoped GaAs spacer layer is used on the anode side to produce a depletion region of length W , much longer than the thickness of the quantum well region l . The transit-time through this layer is much larger than that through the quantum well region; this device forms a quantum well injection transit-time (QWITT) diode.

(b) Small-signal equivalent circuit for the structure shown in (a). Z_{QW} is the specific impedance, ϵ' is the effective dielectric constant, and σ is the injection conductance, of the quantum well; Z_{tt} is the specific impedance, and ϵ is the dielectric constant of the depletion region. R_{prstc} represents the parasitic series resistance due to any undepleted spacer regions, highly doped contact regions, and ohmic contacts.

where ϵ' is the effective dielectric constant of the injection region. The total small-signal specific impedance (excluding parasitic elements) of the QWITT diode is the sum of this specific impedance and that of the depleted spacer region Z_{tt}

$$Z = Z_{QW} + Z_{tt} \quad (3) \quad (2.3)$$

To obtain the transit-time specific impedance Z_{tt} , charge transport through the depleted (drift) region must be considered. Here it is assumed that the depletion region electric field is high enough to cause injected charge to traverse the depletion region at a constant saturated velocity v_s . Although this approximation will break down for extremely thin depletion regions in which transient transport effects may be significant, it should be adequate in establishing trends of device operation. The influence of transient transport effects will be discussed in Section 2.3 after the basic results are established.

Use of a frequency-independent injection conductance and a constant saturation drift velocity permits the application of analytical methods previously established for other transit-time devices [53-55]. Based on these results, we can integrate the drift region electric field to obtain the specific impedance at an angular frequency ω for this device as

$$Z_{tt} = \frac{W}{j\omega\epsilon} \left[1 - \frac{\sigma}{\sigma + j\omega\epsilon} \frac{1 - \exp(-j\theta_d)}{j\theta_d} \right] \quad (4) \quad (2.4)$$

where ϵ is the dielectric constant of the drift region, and θ_d is the drift angle, given by $\theta_d = \omega W/v_s$. For simplicity the dielectric constant of the quantum well region and the drift region have been assumed to be equal in this case. The transit-time specific negative resistance that can be obtained from the depleted spacer region is the real part of (2.4):

$$R = \frac{2 \left(\frac{v_s \epsilon}{2\sigma^2} \right)}{\left(\frac{\omega}{\sigma/\epsilon} \right)^2 \left[1 + \left(\frac{\omega}{\sigma/\epsilon} \right)^2 \right]} \left[1 - \cos \left(\frac{\omega W}{v_s} \right) + \frac{\omega}{\sigma/\epsilon} \sin \left(\frac{\omega W}{v_s} \right) \right] \quad (2.5)$$

where σ is given by (2.1). The specific resistance of the quantum well injection region given by the real part of (2.2) is

$$R_{QW} = \frac{\frac{l}{\sigma}}{1 + \left(\frac{\omega}{\sigma/\epsilon} \right)^2} \quad (6) \quad (2.6)$$

The total specific resistance of a QWITT diode (excluding parasitic resistance in the device) is given by the sum of (2.5) and (2.6). In conventional transit-time devices the injection conductance is positive, yielding a positive injection resistance, which must be overcome by a drift region negative resistance. For a quantum well injection region σ can be negative, and thus the possibility of a negative injection conductance is introduced. In this case the resistance of both the transit-time region and the injection region may be negative.

2.2 Small Signal Characteristics

Examination of (2.5) and (2.6) shows that in virtually all cases of interest the specific negative resistance of a QWITT diode is dominated by the drift region specific negative resistance (see Appendix 1). Equation 2.5 then provides a good

approximation to the total specific negative resistance of the entire structure; therefore, this section focuses on this equation.

2.2.1 Injection Conductance and Transit Angle Optimized Characteristics

As expected for a transit-time device, there is a specific length of the depletion region W which yields the maximum negative resistance for any given frequency, injection conductance, and saturation velocity. The optimum length is found by solving the equation $\partial R/\partial W = 0$, which yields

$$\tan\left(\frac{\omega W}{v_s}\right) = -\frac{\omega \epsilon}{\sigma} \quad (7) \quad (2.7)$$

When using (2.7) it is necessary to select the appropriate branch of the inverse tangent function. For σ positive, (2.5) yields a negative resistance only for the $(2\pi - \pi/2, 2\pi + \pi/2)$ branch. For σ negative, the $(-\pi/2, \pi/2)$ branch of the inverse tangent function should be used. At any given frequency there is also an optimum value of injection conductance σ , which is obtained from the solution of the equation $\partial R/\partial \sigma = 0$. This optimum quantum well injection conductance is given by

$$\left| \sigma_{\text{opt}} \right| = \frac{\omega \epsilon}{\sqrt{3}} \quad (8) \quad (2.8)$$

Thus, at a particular operating frequency there is a unique combination of injection conductance σ and drift region length W which provides the maximum small-signal negative resistance for the device. For such an optimized device, the specific negative resistance is given by

$$R_{\text{opt}} = - \frac{v_s}{4\epsilon\omega^2} \quad (2.9)$$

The solid line in Fig. 2.2 shows the envelope of maximum negative resistance that can be obtained from QWITT-type devices. The expression in (2.9), which applies for both positive and negative injection conductance, indicates two important results: (a) the fully optimized specific negative resistance falls off as $1/\omega^2$, and (b) the maximum available negative resistance is directly proportional to the carrier velocity, v_s , in the drift region.

The importance of choosing an optimum W is well known from the general theory of transit-time devices. However, the importance of optimizing the injection conductance σ has not been widely recognized. The ability to engineer σ by means of quantum well design provides the QWITT diode with an advantage over other transit-time diodes, such as BARITTs (barrier injection transit-time diode [56]) and TUNNETTs (tunnel injection transit-time diode [57]), whose ranges of available injection conductance are more constrained. It should be noted that even for these devices, optimization of σ should still allow improvement in BARITT and TUNNETT design.

2.2.2 *Transit Angle Optimized Characteristics*

Since it may not always be possible to adjust the quantum well injection region conductance σ in accordance with (2.8), it is useful to examine the behavior of (2.5) for fixed σ . When (2.7) is used to determine the optimum depletion region

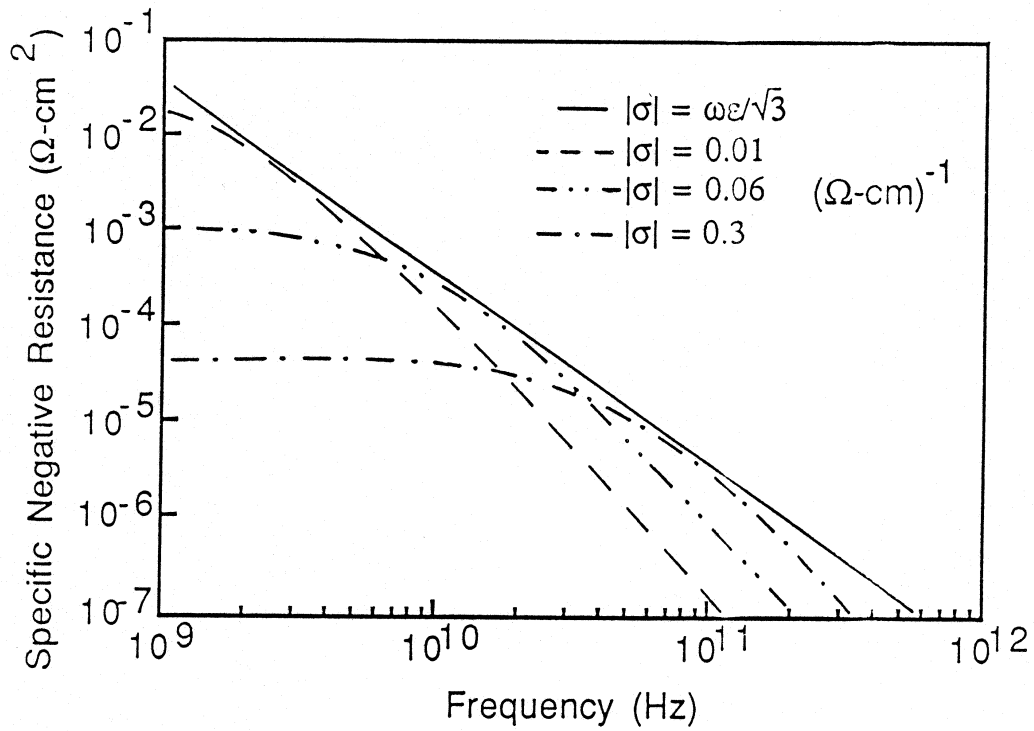


Fig. 2.2: Transit angle optimized small-signal specific negative resistance curves for fixed values of quantum well injection conductance (dashed curves, given by (2.5)), and the performance envelope for both injection conductance and transit angle optimization (solid curve, given by (2.9)). The depletion region is assumed to be GaAs, with a saturation velocity v_s of 6×10^6 cm/sec. The optimized depletion layer thickness corresponding to each point on the curves is found from (2.7); for the solid curve the injection conductance σ at each frequency is found from (2.8), and the transit angle is $\pi/3$.

length as a function of frequency, the behavior of (2.5) becomes independent of the sign of σ . Although the frequency dependent behavior of a fixed device structure (i.e., one with fixed W and σ) is very sensitive to the sign of σ (see below), a device with a properly optimized depletion length W yields the same small-signal negative resistance at its design frequency, regardless of whether σ is negative or positive. Figure 2.2 shows the maximum negative resistance possible for several values of $|\sigma|$ and also shows that all curves for constant σ fall under the envelope given by (2.9). The parameter $\omega_0 = |\sigma|/\epsilon$ represents an important characteristic angular frequency for these devices. For $\omega \ll |\sigma|/\epsilon$, the maximum specific negative resistance R_m is given by

$$R_m = -\frac{v_s \epsilon}{2\sigma^2} \quad (10)$$

(2.10)

When $\omega \gg |\sigma|/\epsilon$, the maximum negative resistance as a function of frequency is given by

$$R_m = -\frac{|\sigma| v_s}{\epsilon^2 \omega^3} \quad (11)$$

(2.11)

For low frequencies (i.e., $\omega \ll |\sigma|/\epsilon$), the negative resistance decreases as the quantum well injection conductance is made larger. However, the high frequency performance of a QWITT diode improves as the injection conductance increases, i.e. to obtain good high frequency performance, the quantum well should be designed so that the slope of its J-V curve is large.

2.2.3 Positive Injection Conductance Characteristics

For a device with both fixed injection conductance and fixed depleted spacer layer length the behavior of (2.5) is very sensitive to the sign of the injection conductance. For positive σ the device behaves much like a BARITT or TUNNETT diode. In this case a band-limited negative resistance is obtained from the drift region. As noted earlier, optimum performance at a frequency ω is obtained using an injection conductance $\sigma = \omega\varepsilon/\beta$ (2.8) and a transit angle of $5\pi/3$ (2.7) (giving $W = 5\pi v_s/3\omega$). For a fixed value of σ , (2.10) and (2.11) give the available negative resistance for $\omega \ll \sigma/\varepsilon$ and $\omega \gg \sigma/\varepsilon$. In the low frequency case (2.7) yields an optimum transit angle of 2π , giving a depletion region length W of $2\pi v_s/3\omega$. At high frequencies (i.e., $\omega \gg \sigma/\varepsilon$) the optimum transit angle is $3\pi/2$, corresponding to a length W of $3\pi v_s/2\omega$. Thus, for a given value of positive σ , the optimum transit angle varies from 2π at low frequencies to $3\pi/2$ at high frequencies, with completely optimized performance for a transit angle of $5\pi/3$ at a frequency ω of $\sqrt{3}\sigma/\varepsilon$. Typical band-limited negative resistance versus frequency characteristics for several values of W are shown in Fig. 2.3, along with the envelopes given by (2.9-2.11).

For this mode of operation a quantum well injection region is not required; tunneling through a single barrier could be used instead. The preceding analysis is valid for such a device with the use of an appropriate positive value of injection conductance σ .

2.2.4 Negative Injection Conductance Characteristics

The situation for negative σ , i.e. at the bias point for which the quantum well exhibits negative differential resistance, has not previously been analyzed in the

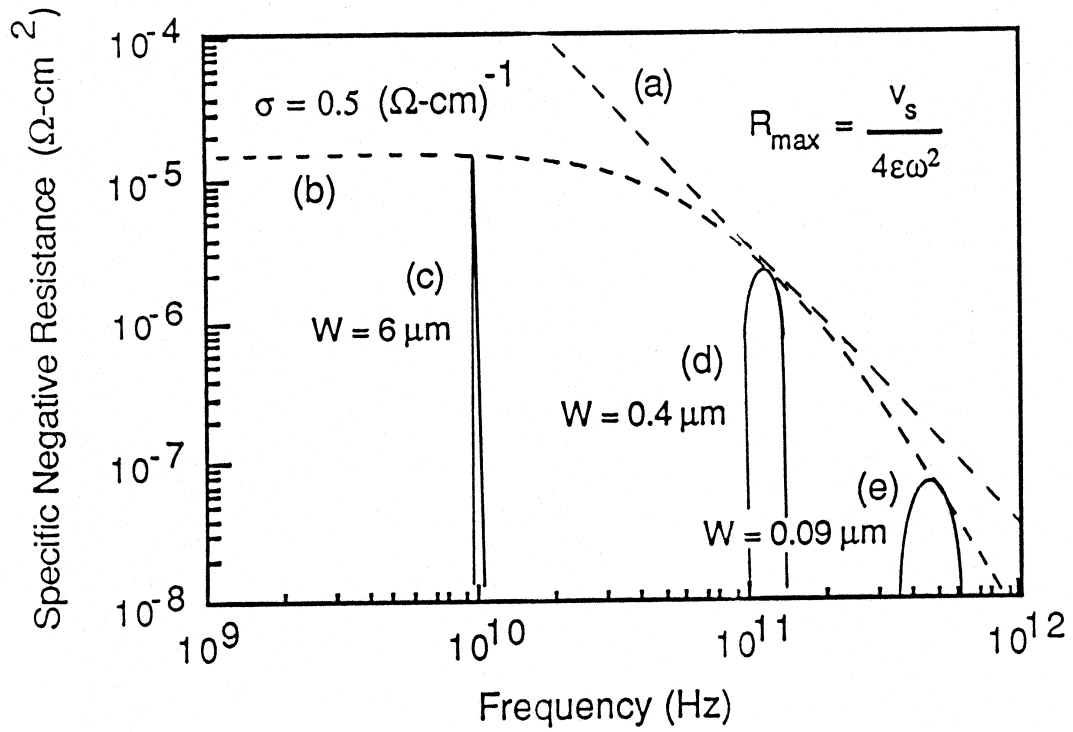


Fig. 2.3: (a) Injection conductance and transit angle optimized envelope of specific negative resistance, given by (2.9); (b) transit angle optimized specific negative resistance for devices with a positive quantum well injection conductance σ of $0.5 \Omega^{-1}\text{cm}^{-1}$, given by (2.5) and (2.7); and band-limited characteristics for devices with fixed depletion layer thicknesses W of (c) $6.0 \mu\text{m}$, (d) $0.4 \mu\text{m}$, and (e) $0.09 \mu\text{m}$, given by (2.5).

transit-time literature. The specific negative resistance R of a QWITT diode as a function of ω again exhibits distinctly different behavior for $\omega > |\sigma|/\epsilon$ and $\omega < |\sigma|/\epsilon$. For $\omega \ll |\sigma|/\epsilon$, R is a constant from dc up to $\omega = |\sigma|/\epsilon$ and is given by

$$R \cong \frac{W}{\sigma} + \frac{W^2}{2\epsilon v_s} \quad (2.12)$$

The second term in (2.12) is always positive and represents the space-charge resistance familiar in the theory of conventional transit-time devices. Overall, R is negative if σ is negative and W is sufficiently small ($W < 2\epsilon v_s/|\sigma|$). Thus, for low frequencies, when transit time effects in the depletion region are not important and when the injection conductance σ is negative, the resulting negative resistance is broadband and independent of frequency. From (2.12) a maximum negative resistance of $-v_s\epsilon/2\sigma^2$ (equal to that predicted by (2.10)) is obtained for $W = v_s\epsilon/|\sigma|$. Examination of (2.7) for $\omega \ll |\sigma|/\epsilon$ shows that the optimum transit angle is proportional to the angular frequency ω

$$\theta_d (\sigma < 0, \omega \ll |\sigma|/\epsilon) \cong \frac{\omega}{|\sigma|/\epsilon} \quad (2.13)$$

Thus the optimum depletion layer thickness for low frequencies is independent of frequency and is equal to $v_s\epsilon/|\sigma|$. The frequency-independent negative resistance and optimum depletion region length exhibited here is a new feature for a transit-time device and is never seen for cases in which the injection conductance is positive.

For $\omega \gg |\sigma|/\epsilon$ and $\sigma < 0$ the optimum transit angle (from (2.7)) is no longer frequency dependent (as it is for the low frequency case above), but approaches $\pi/2$ for high frequencies, corresponding to a depletion region length of $W = \pi v_s/2\omega$. Thus, for a given value of negative σ , the optimum transit angle

varies from $\omega\varepsilon/|\sigma|$ at low frequencies (i.e., $\theta_d \ll 1$) to $\pi/2$ at high frequencies, with completely optimized performance for a transit angle of $\pi/3$ at a frequency ω of $\sqrt{3}|\sigma|/\varepsilon$ (from (2.7) and (2.8)). For a fixed value of W and σ , as ω is increased just beyond $|\sigma|/\varepsilon$ the device negative resistance rolls off as $1/\omega^3$ (in accordance with (2.11)) and changes from negative to positive at the value ω_c , given by

$$\omega_c \cong \frac{v_s}{2W} \left(\pi + \sqrt{\pi^2 - 8 \frac{|\sigma|W}{\varepsilon v_s}} \right) \quad (2.14)$$

At this frequency the device can no longer oscillate. The intrinsic transit-time cut-off frequency, ω_c , of a given device is thus a function of the length of the depletion region W , the saturation velocity v_s , and the injection conductance of the quantum well. Figure 2.4 illustrates the negative resistance versus frequency characteristics for several values of depletion layer thickness W , assuming a fixed value of negative injection conductance.

2.3 Device Design Considerations

In general, small-signal analysis of the negative resistance of transit-time diodes is useful for establishing oscillation thresholds and hence the structures needed to obtain the highest possible operating frequencies. It does not, however, provide design information for power-optimized structures. This section presents a discussion of: (a) the determination of quantum well injection conductance and its influence on small-signal characteristics; (b) realistic estimates of maximum oscillation frequencies for these devices; and (c) the performance of QWITT diodes in comparison to other transit-time devices.

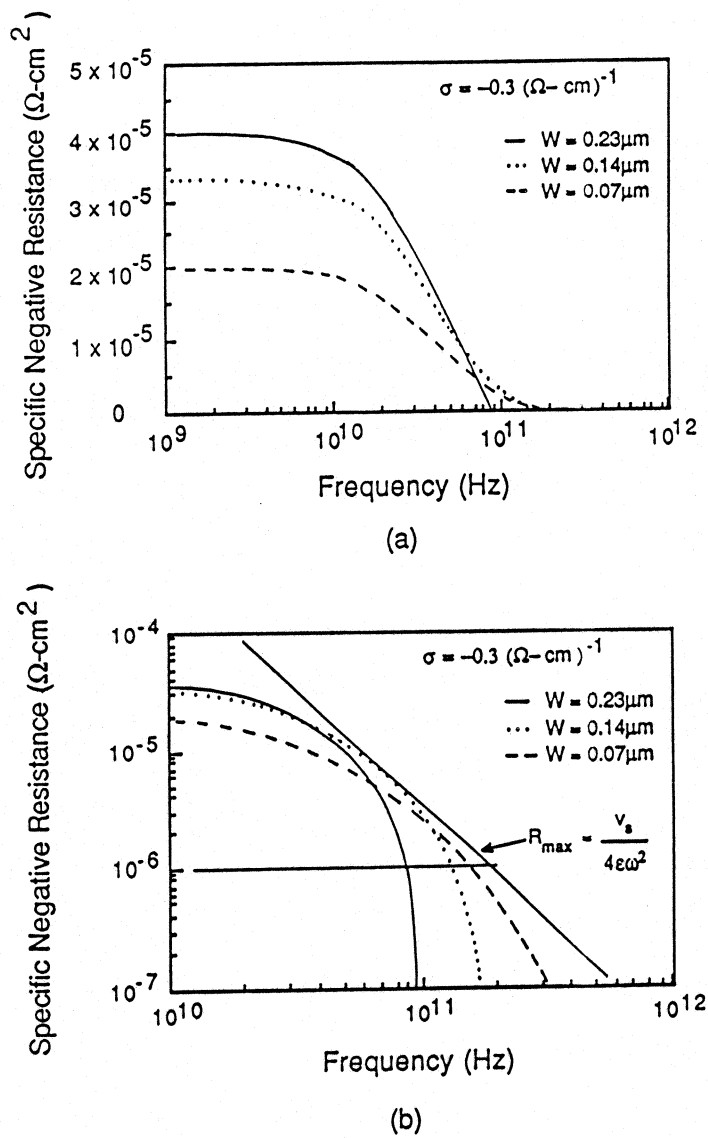


Fig. 2.4: Specific negative resistance for devices with a negative injection conductance σ of $-0.3 \Omega^{-1}\text{cm}^{-1}$ and depletion layer thicknesses of $0.23 \mu\text{m}$, $0.14 \mu\text{m}$, and $0.07 \mu\text{m}$. For such a device $|\sigma|/\epsilon = 41 \text{ GHz}$.

(a) Semi-logarithmic scale emphasizing the low frequency ($f \ll 41 \text{ GHz}$) behavior of these devices. For low frequencies the specific negative resistance is given by (2.10), and is frequency independent.

(b) Log-log scale emphasizing the high frequency ($f \gg 41 \text{ GHz}$) behavior of these devices. For high frequencies the device resistance changes from negative to positive at the intrinsic transit-time cut-off frequency, given by (2.14). A more realistic estimate of cut-off frequency is obtained by finding the intersection of the device specific negative resistance curve and a curve of constant specific contact resistance, shown at $10^{-6} \Omega\text{-cm}^2$.

2.3.1 Quantum Well Injection Conductance

This small-signal analysis clearly indicates the influence of the quantum well injection conductance σ (i.e., $l \partial J_{\text{QW}} / \partial V_{\text{QW}}$) on the performance of a QWITT diode. Unfortunately, at present there are no generally accepted, accurate theoretical models which predict the transport behavior (and hence σ) of quantum well structures. However, it is possible to estimate the value of σ using the dc J-V characteristics of quantum well diodes. To apply (2.1), the current density through the device must be obtained as a function of the voltage dropped across the quantum well region only. Thus, terminal J-V characteristics must be corrected for any voltage drops across depletion and contact regions. Examination of both experimental and theoretical results in the literature [58, 61, 63, 64] indicates that for a wide variety of quantum well structures, when biased to produce negative differential resistance, the room temperature value of σ lies between about $-0.05 \Omega^{-1}\text{cm}^{-1}$ and $-0.5 \Omega^{-1}\text{cm}^{-1}$, with an average value of about $-0.3 \Omega^{-1}\text{cm}^{-1}$. To obtain large values of injection conductance, the magnitude of the current density is more important than the peak-to-valley current ratio for the quantum well. For instance, quantum well structures with large peak-to-valley ratios but lower current density [58] yield lower values of σ than that obtained from structures with higher current density but lower peak-to-valley ratios [58-60]. This large current density is related to the use of thin quantum well barriers; in some cases [59, 60] the barriers are more than a factor of two thinner than other structures [58].

It is illuminating to consider the small-signal behavior of a QWITT device with a typical injection conductance of $-0.3 \Omega^{-1}\text{cm}^{-1}$. Figure 2.4 shows the calculated small-signal negative resistance for this value of σ and several different

values of W , assuming a constant saturation velocity v_s of 6×10^6 cm/sec. The specific negative resistance in each case is constant below $|\sigma|/\epsilon$, which is 41 GHz here. As noted earlier, the largest negative resistance possible for fixed injection conductance occurs at the frequency $\sqrt{3}|\sigma|/\epsilon$ with a transit angle of $\pi/3$. For $\sigma = -0.3 \Omega\text{-cm}^{-1}$ this maximum negative resistance occurs at 71 GHz for $W = 0.14 \mu\text{m}$. Thus, only the curve for $W = 0.14 \mu\text{m}$ touches the envelope of maximum negative resistance given by (2.9). As expected, when the frequency is increased beyond $|\sigma|/\epsilon$, the specific resistance changes abruptly from negative to positive at the intrinsic transit-time cut-off frequency ω_c (2.14). For a depletion region length $W = 0.23 \mu\text{m}$ this frequency is 94 GHz, while for $W = 0.07 \mu\text{m}$ the intrinsic cut-off frequency is much higher, around 400 GHz. A more realistic estimate of cut-off frequency is obtained by requiring that the specific negative resistance from the device be greater than the specific contact resistance to the device. The contact-resistance related cut-off frequencies for devices with fixed depletion region lengths can be estimated from Fig. 2.4. For $W = 0.23 \mu\text{m}$ the specific negative resistance is greater than a typical contact resistance of 10^{-6} ohm-cm² at frequencies less than 90 GHz, which is quite similar to the intrinsic transit-time cut-off. However, for $W = 0.07 \mu\text{m}$ the contact-resistance related cut-off frequency is around 150 GHz, much lower than the intrinsic transit-time cut-off frequency of 400 GHz.

2.3.2 Maximum Oscillation Frequencies

The small-signal transit-time cut-off frequency given by (2.14) does not consider any impedance matching constraints. The negative resistance available at

the terminals of a device of area A is that of the "intrinsic" device R/A from (2.5), plus the positive resistance associated with any undepleted spacer regions, highly doped contact regions, and ohmic contacts. Note that all these parasitic terms scale with area, so their contributions can be lumped into a parasitic specific positive resistance, R_{prstc} . If r_{circ} is the resistance of the external circuit, then matching constraints require the magnitude of the negative resistance at the terminals of the device to be r_{circ} , i. e.

$$\frac{|R|}{A} = \frac{R_{\text{prstc}}}{A} + r_{\text{circ}} \quad (2.15)$$

Recalling that in the high frequency limit (i.e., $\omega \gg |\sigma|/\epsilon$) the transit-angle optimized specific negative resistance R available from the "intrinsic" device is approximately given by (2.11), the maximum oscillation frequency is

$$\omega_m = \left[\frac{|\sigma| v_s}{\epsilon^2 (R_{\text{prstc}} + A r_{\text{circ}})} \right]^{1/3} \quad (2.16)$$

For a completely optimized QWITT diode, i.e. optimized for both σ and W , the absolute maximum specific negative resistance is given by (2.9). In this case the maximum oscillation frequency ω_m is

$$\omega_m = \frac{1}{2} \sqrt{\frac{v_s}{\epsilon (R_{\text{prstc}} + A r_{\text{circ}})}} \quad (2.17)$$

An upper bound on this frequency is found by requiring that the negative resistance from the device exceed the contact resistance to the device, i.e., $r_{\text{circ}} = 0$ and $R_{\text{prstc}} = R_{\text{cont}}$. Under these conditions, for a typical specific contact resistance of $10^{-6} \Omega\text{-cm}^2$ and saturation velocity of 6×10^6 cm/sec, (2.17) predicts a maximum

oscillation frequency of 180 GHz. In order to achieve such a level of performance, (2.8) would require an injection conductance magnitude of $0.75 \Omega^{-1}\text{cm}^{-1}$, much larger than has been reported in the literature. In addition, the depletion layer length for such an optimized device for $\sigma < 0$ is 55 nm, from (2.7). For such a thin depletion region, transient transport effects may cause carriers to traverse through a part of the depletion region at a much higher velocity than $6 \times 10^6 \text{ cm/sec}$. Examination of (2.17) indicates that increasing the effective saturation velocity may significantly increase the contact-resistance related cut-off frequency. Such effects are discussed further below.

The highest reported oscillation frequency from a quantum well diode is 200 GHz [20]. Examination of the published J-V curve [60] for this device leads to an estimated injection conductance of about $-0.4 \Omega^{-1}\text{cm}^{-1}$. Due to the lightly doped spacer layers used in this device, Brown *et al.* have estimated a depletion layer length of approximately 70 nm at their bias point [60]. Using our small-signal analysis, assuming $W = 70 \text{ nm}$, $\sigma = -0.4 \Omega^{-1}\text{cm}^{-1}$, $v_s = 6 \times 10^6 \text{ cm/sec}$, and $R_{\text{cont}} = 10^{-6} \Omega\text{-cm}^2$, we obtain a contact resistance-limited maximum oscillation frequency of approximately 160 GHz. Considering transient transport effects, an effective saturation velocity of 10^7 cm/sec would yield a cut-off frequency of 212 GHz. Hence, our analysis, allowing for transient transport, is consistent with actual oscillator performance.

The assumption that carrier transport across the depleted spacer region takes place at a constant saturation drift velocity, while useful for establishing functional dependencies, is clearly a poor approximation for depletion region lengths smaller than approximately $0.5 \mu\text{m}$. Transient transport effects such as velocity overshoot

can be significant in such circumstances. The impact of velocity overshoot on the design of transit time diodes has been discussed in the literature [62]. In brief, device performance can be greatly enhanced if overshoot takes place at a favorable point in the RF cycle (near the minimum of the device terminal voltage), but can be degraded if the overshoot takes place at an unfavorable point (near the device terminal voltage maximum). There are as yet no reliable models for transient transport immediately following charge injection through a quantum well. However, it seems likely that some velocity overshoot takes place immediately after injection into the depletion region. In this case the performance of QWITT devices operating in the negative injection conductance mode should be significantly enhanced, while operation in the positive injection conductance mode will be degraded, compared to the constant velocity case treated here. The detailed behavior of the velocity transient subsequent to charge injection is being investigated in our group.

2.3.3 Comparison to Existing Transit-Time Devices

The performance potential of QWITT devices can be compared to other transit-time devices such as BARITT, TUNNETT, and IMPATT diodes. The BARITT and TUNNETT are both positive injection conduction devices. The BARITT suffers from the problem that charge transport around the time of injection involves relatively low velocities. This is an advantage at relatively low microwave frequencies (around X-band), since the low velocity occurs at a favorable point in the RF cycle, i. e. around the time when the magnitude of the device voltage is near a maximum. However, the injected pulse spreads out in the low field region, and this is deleterious to higher frequency performance [22]. As a result BARITT operation

is limited to low millimeter-wave frequencies, and BARITTs are consequently not competitors of QWITT devices at millimeter wave frequencies.

The TUNNETT diode is another positive injection conductance device. It is not clear whether pure large-signal TUNNETT mode operation in homojunction devices is actually achievable under large-signal conditions, since the window in which band-to-band tunneling occurs without impact ionization is rather narrow. This impact ionization tends to degrade the noise performance, but improves the phasing of charge injection. In contrast, pure tunnel injection through quantum wells should be more readily achieved, and the injection conductance may be optimized through appropriate quantum well design. Thus, the positive injection conductance mode of QWITT structures should be superior to single drift pure TUNNETT mode devices.

The most successful transit time device has been the IMPATT diode. Charge injection in IMPATT diodes has a largely inductive admittance [22] which is extremely favorable for obtaining high values of negative resistance. This provides good capability for overcoming the contact resistance, leading to oscillation frequencies in the 200-300 GHz range [23]. However, impact ionization is inherently noisy. It is also an energy-dependent process which ceases to be effective at frequencies associated with the inverse of the energy relaxation time [25], typically in the millimeter or submillimeter-wave frequency range. Compared to impact ionization, tunneling through a quantum well should remain an effective injection process to higher frequencies and should be much less noisy. Whether such potentially higher oscillation frequencies can be obtained with quantum well oscillator/QWITT devices depends critically on the minimum contact and parasitic

series resistances that can be achieved, and the nature of any velocity overshoot that occurs in the QWITT diode.

In summary, in Sections 2.1-2.3 a small-signal analysis of transport through a depletion region has been presented. The analysis indicates that effects associated with the anode side depleted spacer layer dominate design considerations for quantum well oscillator/QWITT diodes [65]. At any particular frequency of operation, achieving maximum performance requires appropriate optimization of both the depleted length of the anode spacer region and the quantum well injection conductance. Appropriate optimization of these parameters is predicted to yield QWITT devices whose RF performance potential is vastly superior to that of bare quantum wells. The major concern in the design of the cathode side spacer layer is minimizing parasitic resistance, so this layer should be as thin as possible while still preventing dopant migration into the quantum well. The structure of the best experimental quantum well oscillators strongly suggests that they are in fact operating in a QWITT mode; additional performance improvements should result from further systematic optimization as suggested by the analysis presented here.

The small-signal analysis also shows that the maximum oscillation frequency of quantum well diode structures will probably be limited by parasitic device elements, such as specific contact resistance and impedance matching constraints. Analytical upper bounds for the maximum oscillation frequency have been obtained. For present state-of-the-art contact technology, the maximum frequency of oscillation can be significantly lower than the intrinsic transit-time cut-off frequency and is much lower than previously suggested frequency limits associated with the characteristic times of resonant tunneling charge injection.

The performance potential of QWITT diodes has been compared to that of other high-frequency transit-time diodes, such as BARITTs, TUNNETTs and IMPATTs. The negative injection conductance mode of the QWITT diode should provide major advantages if significant velocity overshoot takes place immediately following charge injection from the quantum well. Overall, quantum well oscillator/QWITT devices appear to have a niche for low noise applications at millimeter-wave frequencies. Whether or not they can be truly competitive in terms of power and maximum oscillation frequency may depend on the nature and extent of transient transport in the depletion region immediately following injection.

2.4 Large Signal Model

A small signal analysis of the negative resistance of microwave diodes is useful for establishing oscillation thresholds and thus predict the structures needed to obtain the highest possible operating frequencies with the highest specific negative resistance. It does not, however, provide design information for power-optimized structures. Further, if the current through the diode as a function of dc bias and ac voltage across the diode at the fundamental frequency were required, then a large signal model must be developed.

We have developed an analytical large signal model for the QWITT diode. The large signal model [66] uses a piecewise linearized fit to an experimental dc IV characteristic of the quantum well to describe current injection. Using the Ramo-Shockley theorem [32] for transit time effects, a numerical integration of the injected charge pulse over the entire rf cycle is performed to obtain the device current. The

electric field and the carrier velocity in the depletion/drift region are assumed to be constant. Static quantum well I-V characteristics are assumed to be valid at all frequencies. Fourier analysis of the device current then gives the device conductance and susceptance per unit area. Imposing a minimum impedance limit of 1Ω from circuit design considerations, a maximum contact resistance of $10^{-6} \Omega\text{-cm}^2$, and a maximum allowable temperature rise of 200 K, the optimum device area, maximum output power and efficiency are then computed.

At first, we need to find an expression for the total current density as a function of injection angle θ . Consider a particle that is injected at an angle θ from the quantum well into the drift region. If we assume that the electric field in the drift region is large (high bias voltage) then the particle's velocity in the drift region can be assumed to be equal to the saturation velocity of electrons v_s in that region. By the time the particle reaches the contact at the end of the drift region, its phase angle will be $\theta+\theta_d$, where θ_d is the drift angle of the drift region. At angle θ all particles injected from $\theta-\theta_d$ up until θ are still drifting through the device. Hence, we can write

$$Q(t) = \int_{t-t_d}^t J_{QW} dt \quad (2.18)$$

where

$Q(t)$ = Total charge drifting through the device at time t .

$J_{QW}(t)$ = Particle current density through the quantum well at time t .

It is assumed that $J_{QW} = J_{QW}(V_{QW})$ is a known J-V characteristic and that the transient J-V characteristic is approximately equal to the steady state J-V characteristic.

We can change the integration variable as follows

$$\frac{\theta}{2\pi} = \frac{t}{T} = f \cdot t$$

so

$$dt = \frac{1}{2\pi f} d\theta$$

where f is the frequency of operation. Eq.(2.18) can be written as

$$Q(\theta) = \frac{1}{2\pi f} \int_{\theta - \theta_d}^{\theta} J_{QW}(\theta) d\theta \quad (2.19)$$

Using the Ramo - Shockley theorem [32], we can write

$$J(\theta) = \frac{Q(\theta) \cdot v_s}{W} \quad (2.20)$$

where

v_s = saturation velocity of electrons in the drift region

W = length of the drift region

From Eqns.(2.19 & 2.20) we can write

$$J(\theta) = \frac{v_s}{2\pi f W} \int_{\theta - \theta_d}^{\theta} J_{QW}(\theta) d\theta \quad (2.21)$$

and since $\frac{2\pi}{\lambda} W = \theta_d$ and $\lambda = \frac{v_s}{f}$ we get

$$W = \frac{\theta_d v_s}{2\pi f} \quad (2.22)$$

By substituting Eq.(2.22) into Eq.(2.21) we obtain

$$J(\theta) = \frac{1}{\theta_d} \int_{\theta - \theta_d}^{\theta} J_{QW}(\theta) d\theta \quad (2.23)$$

Given $J_{QW}(V_{QW})$, one can calculate $J(\theta)$ by numerical integration of $J_{QW}(V_{QW}(1 + \gamma \sin\theta))$

where it is assumed that

$$V = V_0(1 + \gamma \sin(\theta)) = \text{total voltage across the device} \quad (2.24)$$

$$V_{QW} = V_{QW}^{dc}(1 + \gamma \sin(\theta)) = \text{voltage across the quantum well} \quad (2.25)$$

V_0 = the dc bias across the diode

γ = ac modulation factor

and

$$V_1 = V_0 \gamma \sin(\theta) \quad (2.26)$$

where V_1 is the ac voltage component at the fundamental frequency. Now we can write

$$J_1(\theta) = J_{1s} \sin(\theta) + J_{1c} \cos(\theta) \quad (2.27)$$

where $J_1(\theta)$ is the ac component of current at the fundamental frequency. We can find J_{1s} and J_{1c} from a Fourier analysis as follows

$$J_{1s} = \frac{1}{\pi} \int_0^{2\pi} J(\theta) \sin(\theta) d\theta \quad (2.28)$$

$$J_{1c} = \frac{1}{\pi} \int_0^{2\pi} J(\theta) \cos(\theta) d\theta \quad (2.29)$$

From Eqns. (2.23), (2.28), and (2.29) we get

$$J_{1s} = \frac{1}{\pi\theta_d} \int_0^{2\pi} \sin(\theta) \left[\int_{\theta-\theta_d}^{\theta} J_{QW}(\theta) d\theta \right] d\theta \quad (2.30)$$

$$J_{1c} = \frac{1}{\pi\theta_d} \int_0^{2\pi} \cos(\theta) \left[\int_{\theta-\theta_d}^{\theta} J_{QW}(\theta) d\theta \right] d\theta \quad (2.31)$$

Knowing the Fourier components of the current density we can now calculate the ac and dc power densities (i.e., output power per unit area), device efficiency, and device impedance as a function of frequency. The output power density, P/A , is simply

$$\frac{P}{A} = \frac{V_0 \gamma J_{1s}}{2} \quad (2.32)$$

The dc power density, P_{dc}/A , is

$$\frac{P_{dc}}{A} = \frac{V_0}{2\pi\theta_d} \int_0^{2\pi} (1 + \gamma \sin\theta) \left[\int_{\theta-\theta_d}^{\theta} J_{QW}(\theta) d\theta \right] d\theta \quad (2.33)$$

The device conductance per unit area, G , is the ratio of the in-phase current to the ac driving voltage and is given by

$$G = \frac{J_{1s}}{V_0 \gamma} \quad (2.34)$$

The device susceptance, B , is the sum of the cold capacitor susceptance, B_c , and the particle current susceptance, B_p .

$$B_c = \frac{(2\pi f)^2 \epsilon}{\theta_d v_s} \quad (2.35)$$

and

$$B_p = \frac{J_{1c}}{V_0 \gamma} \quad (2.36)$$

The dc-to-rf conversion efficiency, η , is simply the ratio of the output power density, P/A , and the dc power density, P_{dc}/A .

$$\eta = \frac{P/A}{P_{dc}/A} \quad (2.37)$$

The optimum device area, A , is obtained by imposing the following restrictions: (a) The diode resistance and reactance must be at least 1Ω , and (b) A maximum diode temperature rise of 200 K is permitted. Hence,

$$R = \frac{\rho}{A_\rho} \quad 1 \Rightarrow A_\rho \checkmark \frac{G}{G^2 + B^2} \quad (2.38)$$

$$X = \frac{\chi}{A_\chi} \quad 1 \Rightarrow A_\chi \checkmark \frac{B}{G^2 + B^2} \quad (2.39)$$

where G and B are given by Eqns. 2.34-2.36.

Assuming that the entire input power is dissipated in the heat sink, if ΔT is the permissible rise in temperature, R_T is the thermal resistance of the heat sink, κ is the thermal conductivity of the heat sink, then the input power P_{dc} is given by

$$P_{dc} = \frac{\Delta T}{R_T} = \frac{\Delta T 4\kappa \sqrt{A_T}}{\sqrt{\pi}} \Rightarrow A_T \left(\frac{P_{dc} \sqrt{\pi}}{4\kappa \Delta T} \right)^2 \quad (2.40)$$

Thus, the condition to obtain the optimum device area $A(A_p, A_\gamma, A_T)$ is that Eqns. 2.38-2.40 be satisfied.

2.5 Large Signal Characteristics

Using the expressions for output power, efficiency, and optimum device area derived in the previous section, we can compare the predicted large signal characteristics of the QWITT diode, when biased both below resonance (i.e., $\pi/2$ mode) and above resonance (i.e., $3\pi/2$ mode), to other resonant tunneling diode oscillators.

The large-signal analysis shows that when the quantum well is biased below resonance ($\pi/2$ mode) useful rf output power can be obtained from the device for drift angles between 1.1π - 1.8π with maximum output centered around 1.5π . Similarly, for $3\pi/2$ injection maximum output power is obtained at a drift angle of $\pi/2$, consistent with our small-signal analysis. In order to estimate the output power and efficiency as a function of frequency, we have to assume a value for the rf modulation factor, γ . The ac modulation factor is a strong function of the circuit embedding network and the impedance match between the circuit and diode. Fig. 2.5 shows that the output power at any frequency is linearly dependent on the rf voltage modulation factor, γ , ($\gamma = V_{rf}/V_{dc}$) for values of rf voltage modulation between 0.05-0.25. When the circuit is driven at higher ac voltages, i.e., higher

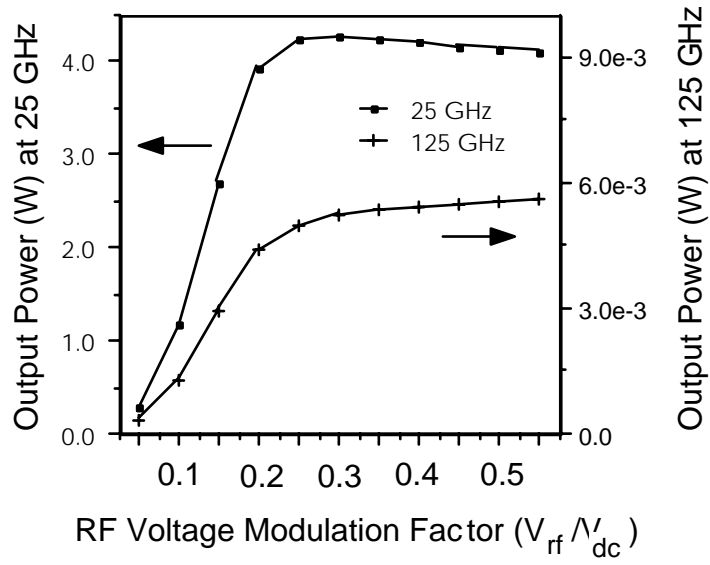


Fig. 2.5: Output power at two representative frequencies as a function of the rf voltage modulation factor for a QWITT diode.

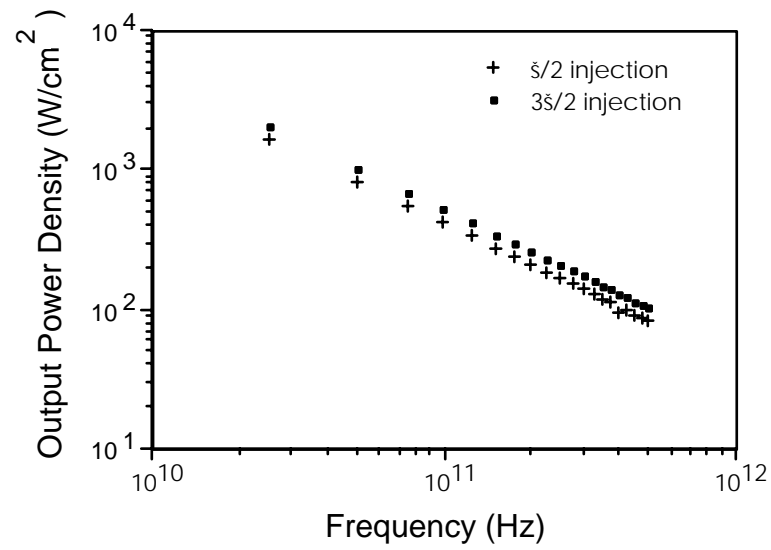


Fig. 2.6: Output power density as a function of frequency for the two bias conditions in a QWITT diode: (a) cross: below the current peak, i.e., below resonance ($\pi/2$ mode); (b) filled square: above the current peak, i.e., above resonance ($3\pi/2$ mode).

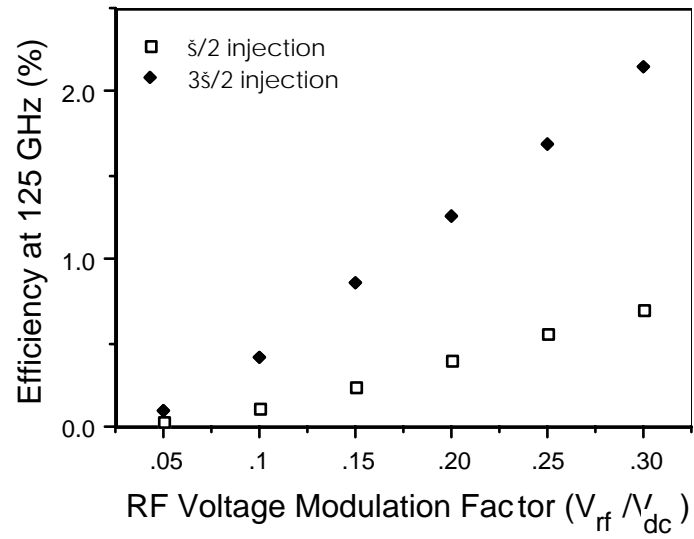


Fig. 2.7: Efficiency as a function of the rf voltage modulation factor at 125 GHz for the two bias conditions for a QWITT diode. (Open squares: $\pi/2$ injection; filled diamonds: $3\pi/2$ injection)

values of γ , the output power starts to saturate. Assuming a value of γ of 0.15, we can calculate the output power density as a function of frequency (Fig. 2.6). The output power density is essentially the same whether the QWITT diode operates in the $3\pi/2$ mode or the $\pi/2$ mode and rolls off as the square of the frequency. However, the improvement in efficiency gained from injecting carriers at $3\pi/2$ operation is significantly higher (Fig. 2.7). The optimum device area as a function of frequency can be estimated by imposing constraints on the device impedance and maximum allowable temperature rise as shown in the previous section (Fig. 2.8). These device areas are then used to obtain the predicted large signal output power as a function of frequency (Fig. 2.8). This large signal model indicates that at 200 GHz the QWITT diode can deliver an output power of around 200 μW , and at 500 GHz, 6 μW output power may be possible (Fig. 2.8). These predicted results are much higher than the best experimental results reported to date of 0.2 μW at 200 GHz [20], primarily due to the use of an asymmetric QWITT structure. We can also study the effect of the intrinsic quantum well characteristics on rf output power. Fig. 2.9 shows that the output power obtained at high frequencies is almost an order of magnitude better when the quantum well injection conductance is increased (i.e., higher peak current density and higher peak-to-valley current ratio). Thus, the intrinsic dc characteristics of the quantum well are crucial in obtaining the maximum output power from a QWITT diode.

In summary, our analyses demonstrate that the QWITT diode should deliver substantially higher power than presently used quantum well oscillators. The analysis techniques used provide practical tools for designing these oscillators for maximum output power and maximum efficiency. The need to obtain an accurate

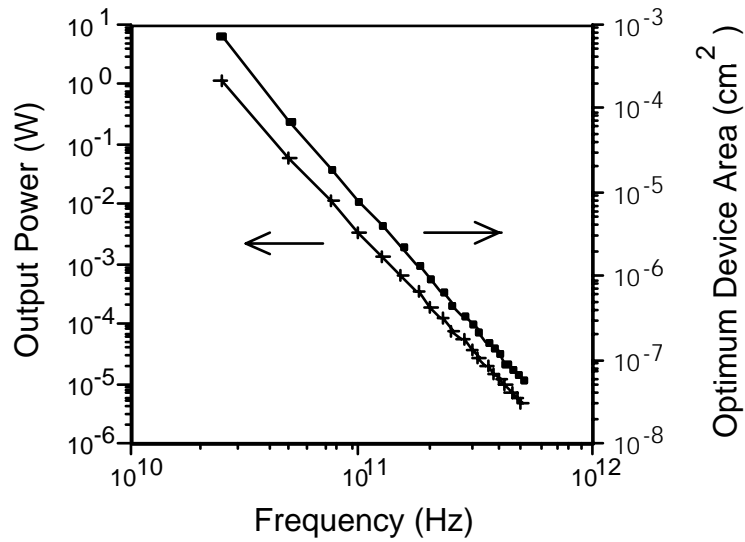


Fig. 2.8: Output power and optimum device area as a function of frequency for a QWITT diode. For the quantum well dc I-V characteristic considered in this analysis, the peak current density is 40 kA/cm^2 at 0.8 V and the current density at the valley is 12 kA/cm^2 at 1.2 V .

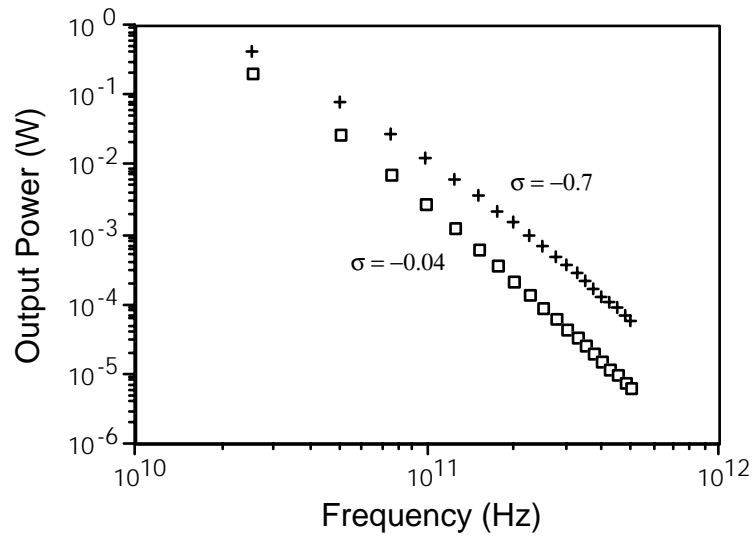


Fig. 2.9: Output power as a function of frequency for two QWITT diodes with different quantum well characteristics (i.e., different values of σ). The dc negative differential resistance for one quantum well was chosen to be much higher than the other.

knowledge of carrier velocity in the drift region in order to predict device performance is emphasized. We have shown that the device parasitics and circuit elements will ultimately limit the maximum oscillation frequency of quantum well oscillators. Beyond 200 GHz the specific contact resistance will become a major performance limiter. In addition, the intrinsic negative resistance dc I-V characteristics of the quantum well must be improved if higher output power is to be obtained from such structures.

In this chapter, small signal and large signal models for the QWITT diode have been developed. These models relate physical device parameters to predicted dc and rf performance. In the subsequent chapters these models will be used to help design optimized QWITT devices for any desired frequency of operation.